IEEE Access
Multidisciplinary | Rapid Review | Open Access Journal

Received April 11, 2021, accepted April 20, 2021, date of publication April 26, 2021, date of current version May 4, 2021.

Digital Object Identifier 10.1109/ACCESS.2021.3075768

The Flexible Smart Traction Power Supply System and Its Hierarchical Energy Management Strategy

YICHEN YING, (Student Member, IEEE), QIUJIANG LIU, (Member, IEEE), MINGLI WU, (Member, IEEE), AND YATING ZHAI, (Student Member, IEEE)
School of Electrical Engineering, Beijing Jiaotong University, Beijing 100044, China

Corresponding author: Mingli Wu (mlwu@bjtu.edu.cn)

This work was supported by the Fundamental Research Funds for the Central Universities under Project 2020JBM067.

ABSTRACT With the increasing requirements of the railway sector for electrified railways and the development of society, the traction power supply system needs to become more flexible, economic and reliable. The traditional traction power supply system has many problems due to its own topology, such as negative sequence current, load fluctuation, low utilization rate of regenerative braking energy, and inability to use the distributed generation along the railway. In order to solve these problems and make the traction power supply system (TPSS) more flexible, efficient and reliable, a novel TPSS called flexible smart traction power supply system (FSTPSS) is proposed. This traction power supply system consists of AC-DC-AC traction substation and the microgrid along the railway. It can effectively mitigate the problems of negative sequence current, improve regenerative braking energy utilization and distributed generation utilization. A hierarchical energy management strategy is also proposed here, which can effectively improve the operating economy of FSTPSS and reduce the load fluctuation of FSTPSS. And based on the actual load measurement power of a traction substation of China's Beijing-Shanghai high-speed railway, the proposed energy management strategy has been verified for the economic improvement and load fluctuation reduction of TPSS.

INDEX TERMS AC-DC-AC traction substation, hierarchical energy management strategy, high-speed railway, microgrid, smart grid, traction power supply system.

I. INTRODUCTION

Traditional traction power supply system (TPSS) has typical problems of asymmetrical power supply and passing the neutral section due to its own structure. Among them, asymmetric power supply will send back a large amount of negative sequence current to the utility power grid, which will easily cause the negative sequence current of public connection point to exceed its standard [1], and increase the power supply cost. Electric locomotives usually generate a large number of harmonics. If these harmonics are directly transmitted to the grid without control, it may cause the harmonics of the utility power grid to exceed the standard. The neutral section makes the traction network set up many phase separation areas, which increases the construction cost of the traction network. When the train passes the neutral section, it will cause voltage and current pikes and transients to TPSS, as well as train speed loss. In recent years, with the development of power electronics technology, some studies propose using AC-DC-AC traction substation to replace traditional traction substation, eliminating neutral section, realizing co-phase power supply across the full line, and solving the problem of power quality in TPSS.

In [2], a traction substation with AC-DC-AC topology based on multi-converter has been proposed, and the operation results show that the AC-DC-AC traction substation can well improve the power quality of TPSS. He *et al.* [3] has proposed a novel co-phase TPSS, and in the proposed system, a DC power transmission system is designed to provide access for distributed generation. In [4], a co-phase TPSS has been built in Meishan, China. The running test results validate the feasibility of the proposed co-phase power supply system. Therefore, it is feasible to replace traditional traction substation with AC-DC-AC traction substation which could effectively improve the power quality in TPSS.

In order to build a more environmentally friendly TPSS and reduce the operating cost of TPSS, the economics of energy storage system for electrified railways is analyzed in [5].

The associate editor coordinating the review of this manuscript and approving it for publication was Alon Kuperman.

Simulation results show that using a suitable energy storage system can effectively improve the economics of traction substation. The research in [6] points out that the microgrid formed by distributed generation and energy storage device along the railway can be connected to the railway traction network to increase the power supply capacity of TPSS. However, after access to distributed generation, the power flow of TPSS will become more difficult to predict due to the randomness of distributed generation output. But if the output of distributed generation and traction load can be accurately predicted, this problem can be solved. Some day-ahead forecasts for photovoltaic are proposed in [7]–[9]. The results show that the day-ahead forecasts for photovoltaic are very accurate on a time scale of minutes. The traction load estimation method is analyzed in [10]–[12]. The analysis results show that although the traction load has a certain degree of randomness, if the appropriate time scale is selected, the load forecast can be very accurate. Therefore, although both traction load and distributed generation output have a certain degree of randomness, the use of appropriate load forecasting technology can still accurately predict them on a certain time scale, thereby facilitating effective energy management system. In [13], [14], the converter control of the energy storage system (ESS) is analyzed in the DC power transmission system. Some simulation models of microgrid interconnection including railways are proposed in [15]–[17]. These simulation results show that railway and microgrid can exchange power stably through converters.

At present, there are some studies devoted to researching novel TPSS and its energy management strategy. M. Chen [18] has proposed a topology scheme of installing hybrid energy storage system (HESS) on DC bus of AC-DC-AC traction substation to collect and utilize regenerative braking energy of train. However, the effect of different train positions on power transmission efficiency was not considered in this study. A centralized-decentralized automation architecture is proposed in [19]. The energy management system (EMS) proposed in this research can balance the contradiction between the central EMS and the decentralized EMS. However, TPSS proposed in this article is still not completely controlled by power electronic devices, and the energy flow of some substations is still uncontrollable. An optimal economic operation optimization method that takes into account the short-term charge and discharge cost of ESS is proposed in [20]. However, the ESS model considered by this method is too complicated with high computation cost. In practical operation, since the short-term random fluctuations of the load are difficult to accurately predict, complex models cannot actually improve the accuracy of optimization. Kleftakis and Hatziargyriou [21] has proposed an optimal control of reversible substations and wayside storage devices in metro railway networks, which can provide a certain reference for the optimal operation of high-speed railway. In [22], [23], some optimal railway operation methods considering wayside ESS have been proposed, but these methods are based on traditional traction substations. In [24]–[26], some optimization methods for microgrid have been proposed, but these methods do not take into account the traction load. In [27], a coordinated approach of dynamically adjusting the load of the controllable rail train and energy storage battery is designed, which uses demand response decision of rail transits system with minimum operational energy. In [28], an integrated electricity-thermal EMS for high-speed railways is proposed, which uses two mode–train operation EMS and station operation EMS to control the power flow. In [29], a hierarchical model predictive control is designed, the energy consumption of the trains is controlled as a lower level and the energy flow of the whole TPSS is controlled as a higher level. In fact, traction load is also a special load, and it is entirely possible to design a microgrid architecture considering the traction load for which the optimization methods described above can be used. Besides, whether it is the wayside microgrid or the AC-DC-AC traction substation, they are fully controlled by power electronic devices. Therefore, it is possible to integrate the wayside microgrid and the AC-DC-AC traction substation to supply power to the traction load. All power electronic devices in the system are managed in a unified manner to realize the joint optimization of the power supply to the traction load. At the same time, TPSS's reliability and economy can be improved. This makes TPSS more flexible and smarter. Based on this, this paper proposes a flexible smart traction power supply system (FSTPSS) which is shown in Fig. 1 and its hierarchical energy management strategy. The contributions and technical novelty of this paper are as follows:

1) A novel topology of traction power supply system is proposed, which is the first time to combine co-phase power supply system and the wayside microgrid which consider the 10kV distribution network load.

2) Due to the long power supply interval of the co-phase power supply system, the calculation time for global optimization of the overall system is very large and error is unacceptable. Thus, the concept of traction power supply system unit is creatively proposed to determine the optimization range of the co-phase power supply system. For a single FSTPSS unit, an economically optimal energy management strategy is proposed to meet the requirements of the FSTPSS unit EMS. The economics of FSTPSS unit after the optimization of the proposed energy management strategy is verified by a practical case.

3) In order to balance the contradiction between FSTPSS's load fluctuation and operation cost, a central energy management strategy is creatively proposed. For multiple FSTPSS units, a multi-objective optimization method called hierarchical sequence method is adopted to realize the energy management of the central EMS. The optimization goal is to minimize the overall fluctuation of the power obtained by the FSTPSS unit from the utility power grid within the allowable range. The load fluctuation of the whole FSTPSS after the optimization of the proposed energy management strategy is also verified by a case study.

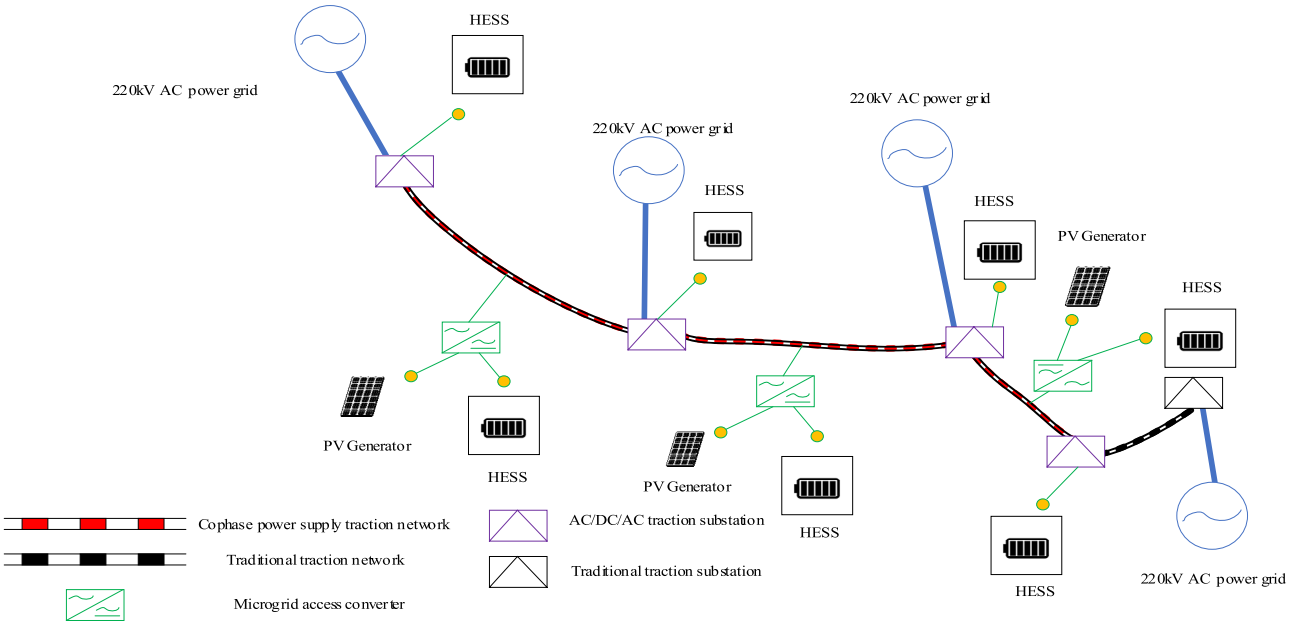

FIGURE 1. Schematic diagram of flexible smart traction power supply system.

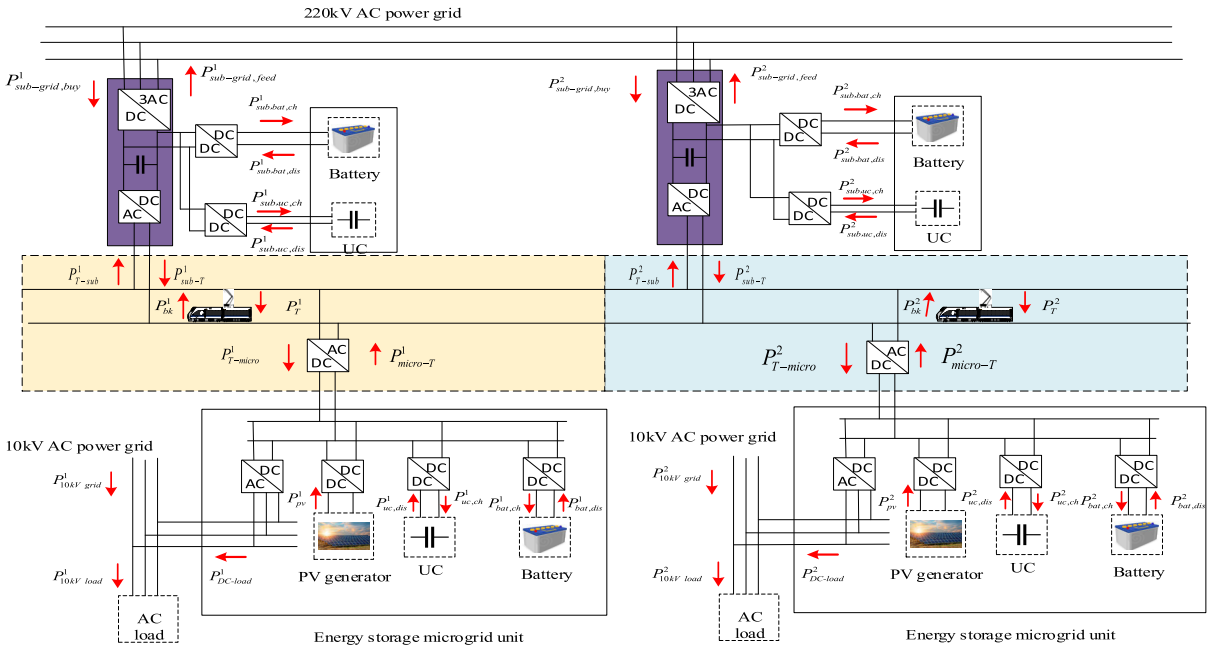

FIGURE 2. Topology diagram of flexible smart traction power supply system.

This paper is organized as follows: Section II introduces the topology of FSTPSS and its power supply mode. Section III introduces the specific implementation steps of the hierarchical energy strategy of FSTPSS. In section IV, the case study and the result are given, followed by the conclusion and the suggestions about future work in Section V.

II. DESCRIPTION OF FLEXIBLE INTELLIGENT TRACTION POWER SUPPLY SYSTEM

The topology of the system is shown in Fig. 2. Compared with TPSS, FSTPSS has the following changes:

First, in FSTPSS, the traditional traction substations are replaced by AC-DC-AC traction substations. This allows the traction substations to achieve symmetrical power supply,

thereby solving the problem of negative sequence current completely. Meanwhile, since each traction substation has realized symmetrical power supply, the system no longer needs the neutral section which is generated to realize the commutation connection. Therefore, TPSS can realize the co-phase power supply in full line. In addition, the DC bus of this AC-DC-AC traction substation is equipped with HESS, so its short-term power supply capacity can be improved. This short-term power supply capacity improvement can effectively meet peak power demand. Also, HESS can collect and store the regenerative braking energy of the locomotive and use it for the next time. In traditional traction substations, this kind of regenerative braking energy is often returned directly to the grid, and there is no return income, sometimes even with penalty costs incurred.

Second, to make better use of all kinds of wayside distributed generation, FSTPSS sets up a 1.5kV DC bus along the railway, which is connected to the traction network through AC-DC converter. The DC bus can be connected to HESS and wayside distributed generation to form regional microgrid. This kind of regional microgrid not only can improve the power supply capacity of traction supply power system and recuperate the regenerative braking energy of the locomotive, but also supply power to the 10kV distribution network near the microgrid to enhance the power supply capacity of the 10kV distribution network. To better improve the voltage level of the traction network, the microgrid connection point of the microgrid should be the lowest point of the network's voltage so that the function of the microgrid can be maximized. Concretely, we could consider every situations of traction network that could happen and calculate every situation's voltage distribution of the traction network. Then, the average voltage distribution could be calculated. The point with the lowest average value could be chosen as our microgrid connection point. Also, this is only a theoretical method of connection point selection. In the actual connection point selection process, the distance between the connection point and the microgrid and the convenience of the point for access also need to be considered.

Since the AC-DC-AC traction substation and the microgrid use fully controllable power electronic converters to connect to the traction network, when the power supply capacity is sufficient, the power source of the locomotive can be completely controlled. Therefore, FSTPSS has extremely high flexibility in power supply strategy selection. This extremely high flexibility allows FSTPSS to select appropriate optimization strategies to reduce the operating cost of FSTPSS, such as buying more electricity when the grid electricity price is low. When the electricity price is high, the pre-stored energy in HESS is preferentially used for power supply, and only when the energy storage device reaches its power supply capacity limit, electricity is taken from the grid. In addition, more power sources also mean that FSTPSS has higher resilience. When the public grid encounters a natural disaster and power failure, or FSTPSS has a power supply failure, the energy control system can timely determine where the

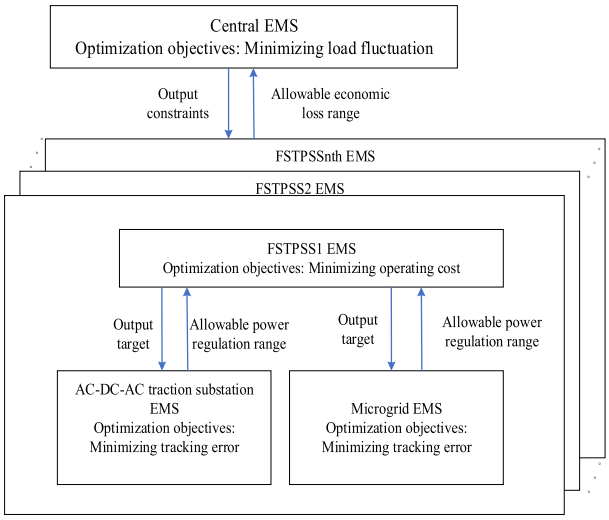

FIGURE 3. Topology diagram of flexible intelligent traction power supply system.

locomotive is located and distribute the power supply near the locomotive to supply power to each locomotive to ensure that the locomotive can continue its service to a safe area. In fact, if this kind of traction power supply system needs to achieve the above-mentioned flexibility and resilience, it also needs a smart energy control system, which can make optimal decisions based on the feedback of various information in the system, such as locomotive power demand, the power generation of distributed generations, and remaining electricity of ESS.

Therefore, FSTPSS is also equipped with a smart energy management system (SEMS), as shown in Fig. 3. At the bottom level are the locomotive EMS, AC-DC-AC traction substation EMS, and microgrid EMS. The middle layer is the FSTPSS unit EMS, which is responsible for regulating the energy flow in the designated power supply interval. The top layer is the central EMS, which is responsible for regulating the energy flow between the units of the FSTPSS. As shown in Fig. 2, the traction substation and microgrid on the left are responsible for power supply in the yellow power supply section, and the traction substation and microgrid on the right are responsible for power supply in the blue power supply section. When the locomotive moves from the blue power supply section into the yellow power supply section, the position sensor sends the locomotive's position information to the central EMS in time, and the central EMS can switch the power supply in time.

III. THE HIERARCHICAL ENERGY STRATEGY OF FSTPSS

FSTPSS's hierarchical energy management strategy is implemented by SEMS. SEMS is a system that manages the energy flow and distribution among AC-DC-AC traction substations, hybrid energy storage systems, high-speed trains, and distributed power sources. SEMS formulates related energy management strategies based on the parameters of locomotive load, distributed generation output, the parameters of hybrid energy storage system, and the parameters of 10kV

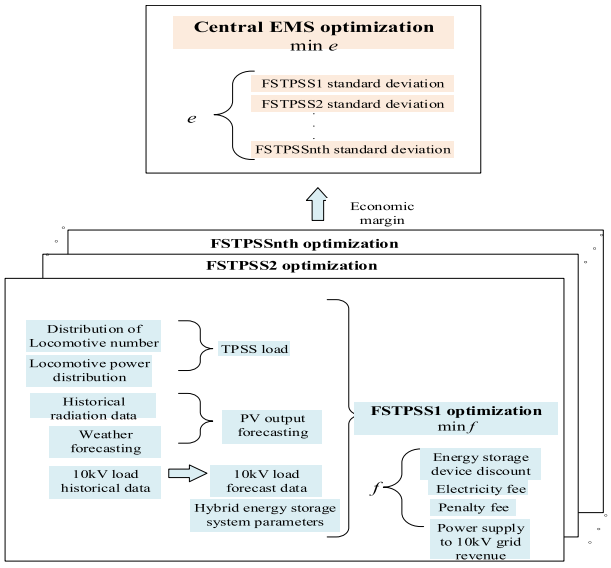

FIGURE 4. Steps of FITPSS's day-ahead energy optimization strategy.

distribution network load. This paper mainly researches the day-ahead energy optimization strategy of FSTPSS. The main steps of FSTPSS's day-ahead energy optimization strategy are shown in Fig. 4.

A. FSTPSS UNIT EMS STRATEGY

For the FSTPSS unit, the daily operating cost should be composed of two parts: one is the cost of the FSTPSS unit getting electricity from the grid every day, and the other is the depreciation cost of HESS of the FSTPSS unit during the daily charge and discharge process. The daily cost of FSTPSS unit obtaining electric energy from the grid usually consists of two parts, one is the electricity consumption cost, and the other is the demand charge which is the penalty for peak load.

The electricity consumption cost refers to the electricity purchased by the FSTPSS unit from the grid multiplied by the unit price of electricity. The calculation formula is shown in (1):

$$C_{ECC} = \sum_{t=1}^{T} \pi_{ECC}^{t} \cdot P_{grid,buy}^{t} \cdot \Delta t/60 \tag{1}$$

where T is the total number of time step in a day, t is the current moment, Δt (min) is the time interval, π_{ECC}^{t} (¥/kWh) is the unit price of electricity, and $P_{grid,buy}^{t}$ (kW) represents the active power from the grid consumed by the FITPSS unit.

The demand electricity cost refers to the maximum average power of the FSTPSS traction transformer within 15 minutes in a day multiplied by the demand electricity price unit price. As shown in (2) and (3):

$$P_{avg}^{t} = \sum_{t}^{t+15/\Delta t-1} P_{grid,buy}^{t}/(15/\Delta t)$$
$$t = 1, 2, \ldots, T - 15/\Delta t + 1 \tag{2}$$

$$C_{DC} = \pi_{DC} \cdot \max(P_{avg}^{1}, P_{avg}^{2}, \ldots, P_{avg}^{T+15/\Delta t-1}) \tag{3}$$

where P_{avg}^{i} is the average active power within 15 min of traction substation, π_{DC}^{t} (¥/kWh) is the unit demand electricity cost.

As the microgrid system along the railway is also connected to the 10kV distribution network, it is also necessary to consider that under certain circumstances, FSTPSS will supply power to the 10kV distribution network. Therefore, the FSTPSS system mentioned in this paper has two aspects of transactions. On the one hand, it is the transaction between FSTPSS and the utility power grid. This part of the transaction complies with the transaction system mentioned above. On the other hand, it is the transaction between the wayside microgrid and the 10kV distribution network. This part of the transaction can use the internal electricity trading mechanism of the microgrid. If the microgrid successfully supplies power to the 10kV distribution network, a certain amount of revenue from electricity sales can be obtained, and the electricity sale revenue is equal to the price of electricity minus the transmission cost of using the distribution network to transmit electricity, as shown in (4):

$$C_{ESR} = \sum_{t=1}^{T} (\pi_{ECC}^{t} - \pi_{trans}) \cdot P_{micro-load}^{t} \cdot \Delta t/60 \tag{4}$$

where $P_{micro-load}^{t}$ (kW)is the active power sold by the microgrid, π_{trans} (¥/kW) represents unit power transmission cost.

The unit transmission cost is determined by the megawatt kilometer method [30]–[33]. The concrete calculation method is shown in (5) - (7):

$$\gamma_{z,i} = \frac{C_{z,i}}{P_{rated,i} L_i} \tag{5}$$

$$R_{trans} = \sum_{i}^{N} (\gamma_{z,i} P_{z,i} L_i) + C_{z,0}, P = P_{z,1} + P_{z,2} + \cdots + P_{z,N} \tag{6}$$

$$\pi_{trans} = R_{trans}/P \tag{7}$$

where $\gamma_{z,i}$ is the transmission cost per megawatt kilometer of line i. $C_{z,i}$ is the transmission cost of line i under rated power. $P_{rated,i}$ is the rated transmission power of line i. L_i is the length of line i. R_{trans} is the transmission cost with a transmission power of P, $P_{z,i}$ is the transmission power of line i, $C_{z,0}$ is the transmission loss of network.

For the depreciation cost of hybrid energy storage system during the daily charging and discharging process [19], the charge of each energy storage device is shown in (5):

$$C_{ESS} = \frac{1}{P_{ESS,rate} \cdot T_a} C_{ESS,cap} \times \frac{r(1+r)^n}{(1+r)^n - 1} \times \sum_{t=1}^{T} (P_{ESS}^{t} \cdot \Delta t) \tag{8}$$

where $P_{ESS,rate}$ (MW) is the rated power of the energy storage device, T_a (h) represents the maximum operating time of the energy storage device in one year, $C_{ESS,cap}$ (¥) represents the investment cost of the energy storage device, r (%/year)

represents the depreciation rate (%/year), n (year) represents the normal service life of the energy storage device, P^t_{ESS} (MW) represents the charge and discharge power of the energy storage device.

Therefore, for a FSTPSS unit, to achieve the lowest daily operating cost (DOC) of the system, it is necessary to reduce its electricity consumption cost, demand charge, and HESS depreciation cost as much as possible, and maximize its electricity sale revenue. The objective function can be expressed in (6):

$$\min C_{DOC} = C_{EEC} + C_{DC} - C_{ESR} + C_{ESS} \tag{9}$$

To achieve the optimization target shown in (6), it is necessary to add the constraints of related variables. The following variables currently exist in the optimization target: the power from the grid consumed by the FSTPSS unit ($P^t_{sub-grid,buy}$), the power returned to power grid by FSTPSS unit ($P^t_{sub-grid,fed}$), the charging power of capacitor in AC-DC-AC traction substation ($P^t_{sub,uc,ch}$), the discharging power of capacitor in AC-DC-AC traction substation ($P^t_{sub,uc,dis}$), the state of charge of the capacitor in AC-DC-AC traction substation ($E^t_{sub,uc}$), the charging power of battery in AC-DC-AC traction substation ($P^t_{sub,bat,ch}$), the discharging power of battery in AC-DC-AC traction substation ($P^t_{sub,bat,dis}$), the state of charge of the battery in AC-DC-AC traction substation ($E^t_{sub,bat}$), the power provided by the AC-DC-AC traction substation to the traction network (P^t_{sub-T}), the power returned by the traction network to the AC-DC-AC traction substation (P^t_{T-sub}), the charging power of capacitor in the microgrid ($P^t_{micro,uc,ch}$), the discharging power of capacitor in the microgrid ($P^t_{micro,uc,dis}$), state of charge of the capacitor in the microgrid ($E^t_{micro,uc}$), the charging power of battery in the microgrid ($P^t_{micro,bat,ch}$), the discharging power of battery in the microgrid ($P^t_{micro,bat,dis}$), the state of charge of the battery in the microgrid ($E^t_{micro,bat}$), the power provided by the microgrid to the traction network ($P^t_{micro-T}$), the power returned by the traction network to the microgrid ($P^t_{T-micro}$), the power from DC bus in the microgrid to 10kV distribution network ($P^t_{DC-load}$), the power supplied by the 10kV distribution network to the 10kV load ($P^t_{10kVgrid}$). The variables above are continuous variables.

To facilitate the calculation, the following variables are added: the state variable of limiting capacitor charge and discharge in AC-DC-AC traction substation ($b^t_{sub,uc}$), the state variable of limiting battery charge and discharge in AC-DC-AC traction substation ($b^t_{sub,bat}$), the state variable of limiting capacitor charge and discharge in the microgrid ($b^t_{micro,uc}$), the state variable of limiting battery charge and discharge in the microgrid ($b^t_{micro,bat}$), the state variable of limiting the direction of power exchange between AC-DC-AC traction substation and the grid ($b^t_{sub-grid}$), state variables of limiting the power exchange between AC-DC-AC traction substation and the traction network (b^t_{sub-T}), state variables of limiting the power exchange between the microgrid and traction network ($b^t_{micro-T}$). The variables above are binary variables.

The constraints of the power balance of the FSTPSS unit are as follows:

$$\begin{aligned} &P^t_{sub-grid,buy} + P^t_{sub,bat,dis} + P^t_{sub,uc,dis} + P^t_{T-sub} \\ &= P^t_{sub,bat,ch} + P^t_{sub,uc,ch} + P^t_{sub-T} + P^t_{sub-grid,fed} \forall t \end{aligned} \tag{10}$$

$$\begin{aligned} &P^t_{pv} + P^t_{micro,bat,dis} + P^t_{micro,uc,dis} + P^t_{T-micro} \\ &= P^t_{micro,bat,ch} + P^t_{micro,uc,ch} + P^t_{micro-T} + P^t_{micro-load} \forall t \end{aligned} \tag{11}$$

$$P^t_{sub-T} + P^t_{micro-T} + P^t_{bk} = P^t_T + P^t_{T-sub} + P^t_{T-micro} \tag{12}$$

$$P^t_{micro-load} + P^t_{10kVgrid} = P^t_{10kVload} \tag{13}$$

where P^t_{pv} is the power of photovoltaic power station; $P^t_{sub-grid,fed}$ is the power returned from the AC-DC-AC traction substation to the grid. P^t_T is the power consumed by the traction load. P^t_{bk} is the regenerative braking power of the traction load. $P^t_{micro-load}$ is the power provided by the microgrid to the load of the 10kV distribution network. $P^t_{10kVgrid}$ is the power of the 10kV distribution network. $P^t_{10kVload}$ is the load power of 10kV distribution network. Equation (7) represents the power balance of the DC bus in the AC-DC-AC traction substation. Equation (11) denotes the power balance of the DC bus of the microgrid. Equation (12) represents the power balance of the traction network. Equation (13) represents the power balance of the 10kV distribution network.

The charging and discharging constraints of energy storage devices are as follows:

$$E^t_{i,j} = (1-\kappa_{i,j})E^{t-1}_{i,j} + \eta^{ch}_{i,j} P^t_{i,j,ch} \Delta t - P^t_{i,j,dis} \Delta t / \eta^{dis}_{i,j} \forall i,j,t \tag{14}$$

$$E^{t=1}_{i,j} = E^{t=end}_{i,j} \forall i,j \tag{15}$$

$$\begin{aligned} 0 \le P^t_{i,j,ch} \le \min(&P^{rate}_{i,j}, (E^{rate}_{i,j} \cdot SOC^{\max}_{i,j} - E^{t-1}_{i,j}) \\ &/(\eta^{ch}_{i,j} \cdot \Delta t)) \quad \forall i,j,t \end{aligned} \tag{16}$$

$$\begin{aligned} 0 \le P^t_{i,j,dis} \le \min(&P^{rate}_{i,j}, (E^{t-1}_{i,j} - E^{rate}_{i,j} \cdot SOC^{\min}_{i,j}) \cdot \eta^{dis}_{i,j} \\ &/\Delta t)) \quad \forall i,j,t \end{aligned} \tag{17}$$

where $\kappa_{i,j}$ is the self-discharge coefficient of energy storage device j of system i. $\eta^{ch}_{i,j}$ and $\eta^{dis}_{i,j}$ are efficiency of charging and discharging of energy storage device j of system i, respectively. $SOC^{\max}_{i,j}$ and $SOC^{\min}_{i,j}$ are the maximum and minimum values of the state of charge of energy storage device j of system i. $P^{rate}_{i,j}$ is the rated power of energy storage device j of system i. i can be AC-DC-AC traction substation or the microgrid along railway. j can be battery or capacitor. Equation (14) indicates that the remaining energy of energy storage device at the current moment is equal to the remaining energy at the previous moment plus (or minus) the energy charged (or discharged) at the previous moment. Also, the initial energy of the energy storage device should be equal to the energy of the energy storage device at the end of the day, as shown in (15). Inequalities (16) and (17) indicate that the charging and discharging power of the energy storage device is restricted by the rated power and the current remaining energy of the energy storage device.

Some variables are divided into two variables to distinguish the direction of the variable, so they cannot exist at the same time. Therefore, the following constraints need to be added:

$$P^t_{i,j,ch} \le P^{rate}_{i,j} \cdot b^t_{i,j}, P^t_{i,j,dis} \le P^{rate}_{i,j} \cdot (1 - b^t_{i,j}) \quad \forall i, j, t \quad (18)$$

$$0 \le P^t_{sub-grid,buy} \le S^{\max}_{sub-grid} \cdot b^t_{sub-grid},$$
$$0 \le P^t_{sub-grid,fed} \le S^{\max}_{sub-grid} \cdot (1 - b^t_{sub-grid}) \quad \forall t \quad (19)$$

$$0 \le P^t_{sub-T} \le S_{sub,converter} \cdot b^t_{sub-T}$$
$$0 \le P^t_{T-sub} \le S_{sub,converter} \cdot (1 - b^t_{sub-T}) \quad \forall t \quad (20)$$

$$0 \le P^t_{micro-T} \le S_{micro,converter} \cdot b^t_{micro-T}$$
$$0 \le P^t_{T-micro} \le S_{micro,converter} \cdot (1 - b^t_{micro-T}) \quad \forall t \quad (21)$$

where $S^{\max}_{sub-grid}$ is the short-circuit capacity at the public connection point. $S_{sub,converter}$ is the capacity of the AC-DC-AC traction substation converter. $S_{micro,converter}$ is the capacity of the microgrid converter. Inequality (18) is the restriction of the charging and discharging state of the energy storage device, which is used to ensure that the energy storage device is only in one state of charging and discharging in a period of time. Inequalities (16-18) are the restriction on the power exchange, which guarantee the exchange power between the AC-DC-AC traction substation and the grid, the exchange power between the AC-DC-AC traction substation and the traction network and the exchange power between the microgrid and the traction network can only be in in one of the states of taking power and feeding power.

Finally, the relevant constraints of the 10kV distribution network are as follows:

$$-S_{micro-load,converter} \le P^t_{micro-load} \le S_{micro-load,converter} \forall t \quad (22)$$

$$0 \le P^t_{10kV\,grid} \le S^{\max}_{10kV\,grid} \forall t \quad (23)$$

where $S_{micro-load,converter}$ is the capacity of the converter responsible for power transmission between the microgrid and the 10kV distribution network. $S^{\max}_{10kV\,grid}$ is the short-circuit capacity of the 10kV distribution network. Inequality (22) represents that the power exchange between the microgrid and the 10kV distribution network cannot exceed the upper limit of its converter capacity. Inequality (23) denotes that the power output by the 10kV distribution network cannot exceed its own short-circuit capacity.

B. CENTRAL EMS STRATEGY

For the central EMS, the optimization goal is to minimize the impact of each FSTPSS unit on the grid, so the sum of the standard deviations of the power exchanged by each FSTPSS unit with the grid is selected as the objective function of the central EMS, as shown in (24):

$$\min STD = \left[\sum_{t=1}^{T} \left(\sum_{n=1}^{N} (P^{Rail}_n(t) - P^{Rail}_{av}) \right)^2 / T \right]^{\frac{1}{2}} \quad (24)$$

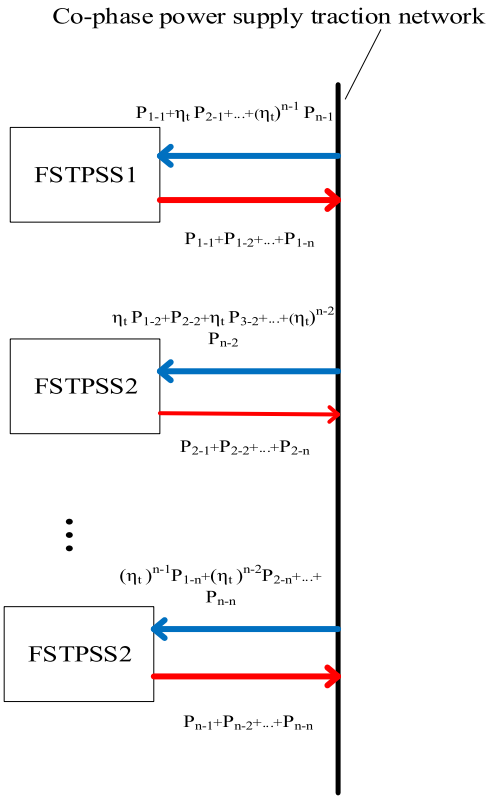

FIGURE 5. Schematic diagram of power exchange between FSTPSS units.

where $P^{Rail}_n(t)$ is the power exchanged between the nth FITPSS unit and the grid at time t, which is equal to $P^t_{sub-grid,buy}$ minus $P^t_{sub-grid,fed}$. N is the number of FSTPSS units managed by the central EMS. P^{Rail}_{av} is the daily average value of the power exchanged between all FSTPSS units managed by the central EMS and the grid, which can be calculated by (25):

$$P^{Rail}_{av} = \sum_{n=1}^{N} \sum_{t=1}^{T} P^{Rail}_n(t) \quad (25)$$

Since the traction network of FSTPSS is a co-phase power supply traction network, the traction network can be equivalent to an AC bus, and the power exchange between each FSTPSS unit is completed through the traction network, as shown in Fig. 5.

In the above, when considering the power exchange in the FSTPSS unit itself, its power transmission loss is ignored since its power transmission distance is very short. For the power transmission between different FSTPSS units, the transmission distance is relatively long (usually a traction power supply section is between 20∼50km), so such power transmission loss cannot be ignored. Therefore, for the power transmission between different FSTPSS units, the transmission efficiency should be considered. If it is assumed that the length (distribution line distance) of the power supply area under each FSTPSS unit is approximately the same, the equation shown in (26) is established to express the relationship

of power exchange between FSTPSS units:

$$\begin{cases} P^1_{sub-T} + P^1_{micro-T} + P^1_{bk} = P_{1-1} + P_{1-2} + \cdots + P_{1-n} \\ P^1_{T-sub} + P^1_{T-micro} + P^1_T = P_{1-1} + \eta P_{2-1} \\ +(\eta)^2 P_{3-1} + \cdots + (\eta)^{n-1} P_{n-1} \\ P^2_{sub-T} + P^2_{micro-T} + P^2_{bk} = P_{2-1} + P_{2-2} + \cdots + P_{2-n} \\ P^2_{T-sub} + P^2_{T-micro} + P^2_T = \eta P_{1-2} \\ +P_{2-2} + \eta P_{3-2} + \cdots + (\eta)^{n-2} P_{n-2} \\ \cdots \\ P^n_{sub-T} + P^n_{micro-T} + P^n_{bk} = P_{n-1} + P_{n-2} + \cdots + P_{n-n} \\ P^n_{T-sub} + P^n_{T-micro} + P^n_T = (\eta)^{n-1} P_{1-n} \\ +(\eta)^{n-2} P_{2-n} + \cdots + P_{n-n} \end{cases} \tag{26}$$

where P^i_{sub-T}, P^i_{T-sub}, $P^i_{micro-T}$, and $P^i_{T-micro}$ are the power exchange variables of FSTPSS i, which are described above. P^i_T is the power consumed by the traction load of FSTPSS i. P^i_{bk} is the regenerative braking power of the traction load of FSTPSS i. P_{i-j} represents the power provided by FSTPSS unit i to FSTPSS unit j. $i, j \in \alpha = \{1,2, \ldots, n\}$. η is the power transmission efficiency between adjacent FSTPSS units. It should be noted that when performing the optimization strategy of the central EMS, the equation (12) in the FSTPSS unit EMS strategy should be replaced by the corresponding equation in (26).

Besides, the optimization goals of the central EMS and the FSTPSS unit EMS are not consistent, so the problem of optimization priority will occur during optimization. For the research of this paper, the economic optimization goal of FSTPSS unit should be guaranteed first, and then the optimization goal of minimizing power fluctuation of each FSTPSS unit could be considered. Therefore, the hierarchical sequence method is proposed to solve the multi-objective optimization problem of this paper. The basic idea of the hierarchical sequence method is as follows: when optimizing multiple goals, divide the priority of each optimization goal. First, the goal with higher priority is optimized, with a certain tolerance set after obtaining the optimal value of the target with higher priority. Then the optimization of the next priority target is performed near the tolerance of the previous target. Its outline is as follows:

$$\begin{aligned} f_1(x^{(1)}) &= \min_{x \in R} f_1(x), \\ f_2(x^{(2)}) &= \min_{x \in R_1} f_2(x), \ R_1 = \left\{ X \,|\, f_1(x) < f_1(x^{(1)}) + m_1, x \in R \right\}, \\ f_3(x^{(3)}) &= \min_{x \in R_2} f_3(x), \ R_2 = \left\{ X \,|\, f_2(x) < f_2(x^{(2)}) + m_2, x \in R_1 \right\}, \\ &\cdots\cdots \\ f_n(x^{(n)}) &= \min_{x \in R_{n-1}} f_n(x), \\ R_{n-1} &= \left\{ X \,|\, f_{n-1}(x) < f_{n-1}(x^{(n-1)}) + m_{n-1}, x \in R_{n-2} \right\} \end{aligned} \tag{27}$$

Among them, $f_1(x), f_2(x), \ldots, f_n(x)$ is the n targets to be optimized arranged by priority, and $m_1, m_2, \ldots, m_{n-1}$ is the optimization tolerance of the corresponding upper-level target.

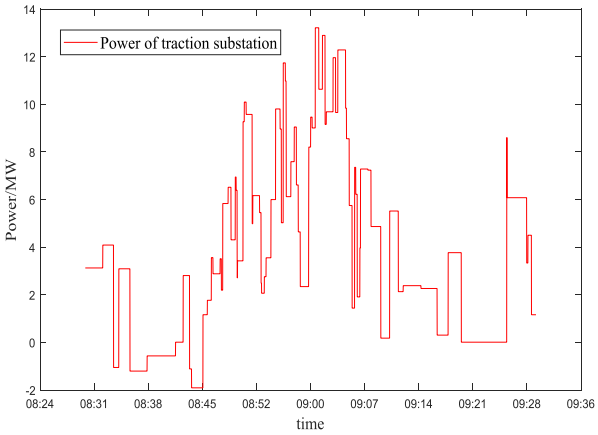

FIGURE 6. Schematic diagram of the generated traction load.

Compared with the use of weights to adjust the priority of multiple goals, the advantage of using the hierarchical sequence method is that there is no need to determine the weight of each goal. For the problem of this paper, it is difficult to draw a weight relationship between each optimization goal, because it is difficult to clarify how much economic benefit each FSTPSS unit needs to sacrifice to minimize the overall power fluctuation of the system. Moreover, for a single FSTPSS unit, its economic benefits are settled separately. If the overall power fluctuation of the system is minimized without considering the economic benefits of a single FSTPSS unit, it is possible that the economic benefits of certain FSTPSS units will drop sharply while the economic benefits of some FSTPSS units remain basically unchanged. This will undoubtedly cause resistance to joint optimization in actual implementation. In this case, this contradiction can be resolved by using the hierarchical sequence method. Each FSTPSS unit gives its own tolerance, that is, the tolerance of economic loss, and then the central EMS optimizes the overall fluctuation of the system. This balances out the contradiction between the economic requirements of a single FSTPSS unit versus the overall power fluctuation of the system.

IV. CASE STUDY

A. CASE STUDY OF FITPSS UNIT EMS

1) CASE DESCRIPTION

In order to verify the effectiveness of the proposed energy management strategy, a high-speed passenger dedicated line on the Beijing-Shanghai high-speed railway is used in this case study. Part of the traction load is shown in Fig. 6 (time interval is 1 second).

In day-ahead load forecasting, the accuracy of load forecasting in an ultra-short period of time is often not very accurate, but the forecasting of the average load in a long period of time is often more accurate [34]. Therefore, when performing day-ahead optimization, a long period of time is usually used as the calculation interval for the average load. So, in the

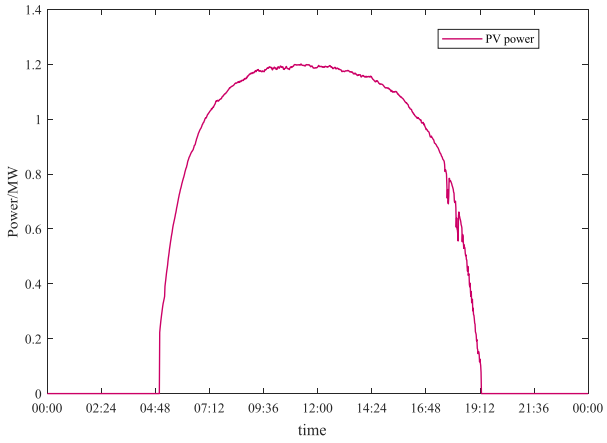

FIGURE 7. Power of PV generation.

day-ahead optimization of this paper, the average load within a time interval of 5 minutes is chosen as the calculation interval. For the load within 5 minutes, the method of real-time optimization and tracking of the target load is used on the same day. After obtaining the average load optimization value within 5 minutes, the method of real-time tracking of the target optimization value is used to optimize the real-time load (time interval is 1 second). The optimization goal of this method is to minimize the error between the real-time load forecast value and the target optimization value in the target time interval.

The solar radiation data of PV plant can be obtained from [35]. The area of the PV panel is 104 m2, the photo-electric efficiency is 15%, and the power of PV generation is shown in Fig. 7.

Lithium iron phosphate battery and UCs are used in ESS. The optimal configuration parameters of batteries and UCs can be obtained by the method in [20] which comprehensively considers their economic benefits to the traction power supply system. The method is as follows: (1) determining the daily investment cost when selecting a pair of PV and HESS capacity;(2) for each selected PV and HESS capacity, calculating the daily electricity cost before and after the installation of PV and HESS (the calculation method of daily power consumption depends on the specific system operation state). (3) Calculating the economic returns which equal to the daily electricity revenue minus the daily investment cost. The daily electricity revenue is equal to the daily electricity cost of the traction power supply system before the installation of PV and HESS minus the daily electricity consumption after the installation of PV and HESS. (4) Repeating steps (1) - (3) several times and finding the PV and HESS capacity with the largest economic returns as the final capacity selection.

The parameters of each energy storage device in the FSTPSS unit are shown in Table 1.

In this paper, the number of lines for the microgrid to supply power to the 10kV distribution network is 1, and the length is set to 10km. Since the transmission network is small, its transmission loss is ignored. The rated power transmission cost can be calculated from [36], which is ¥2.4/hour, and the rated power 0.06MW. Electricity consumption cost, electricity transmission cost and demand electricity cost are shown in Table 2. The load power of the 10kV distribution network is shown in Fig. 10.

TABLE 1. Parameters of energy storage device.

Parameters	Unit	Sub-battery	Sub-UC	Micro-battery	Micro-UC
Rated power	MW	2	5	3	6
Rated capacity	MW h	3	0.3	4.5	0.36
SOC range	/	0.1~0.9	0.05~0.95	0.1~0.9	0.05~0.95
Initial SOC	/	0.5	0.5	0.5	0.5
Self-discharging rate	/month	0.05	0	0.05	0
Efficiency(charge/discharge)	/	0.8/0.8	0.9/0.9	0.8/0.8	0.9/0.9
Operation cost	¥/MWh	23.97	0. 96	23. 97	0.96

TABLE 2. Parameters of electricity costs.

Type	Time ranges	Cost
Electricity consumption cost(¥/kWh)	0:00~6:00 22:00~0:00	0.25
	8:00~12:00 17:00~22:00	1.08
	6:00~8:00 12:00~17:00	0.62
Electricity transmission cost(¥/kWh)	full day	0.04
Demand charge cost(¥/kW)	full day	1.4

2) OPERATION RESULT

The optimization problem of FSTPSS unit is a mixed integer linear programming (MILP) problem, so YALMIP toolbox (version 20200116) is used to write the related objective functions and constraints of the algorithm, and IBM ILOG CPLEX (version 12.10) solver is called to solve MILP problem. The branch-and-cut method is used in solving MILP by CPLEX solver [37]–[40]. The optimization program runs in the MATLAB R2018a under the environment of Intel Core I7-8700 CPU@3.2GHz and 16GB RAM. The comparison of the power obtained by the traction substation from the grid before and after optimization is shown in Fig. 8. It can be seen that the power obtained by the traction substation from the grid is reduced after the optimization, and there is no

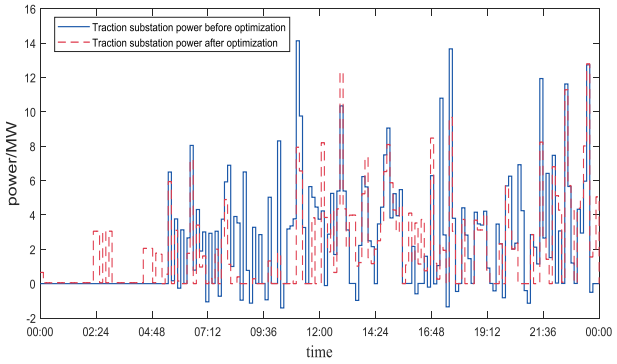

FIGURE 8. Comparison of traction substation power before and after optimization.

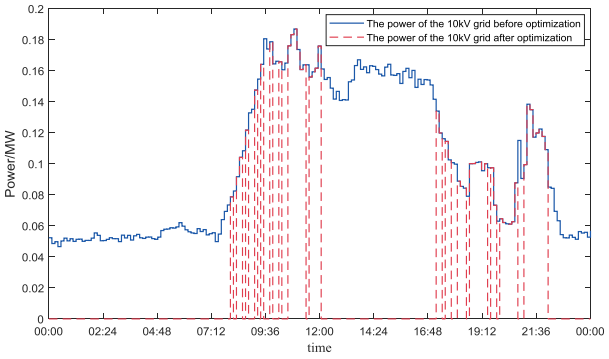

FIGURE 10. Comparison of power consumption of 10kV distribution network before and after optimization.

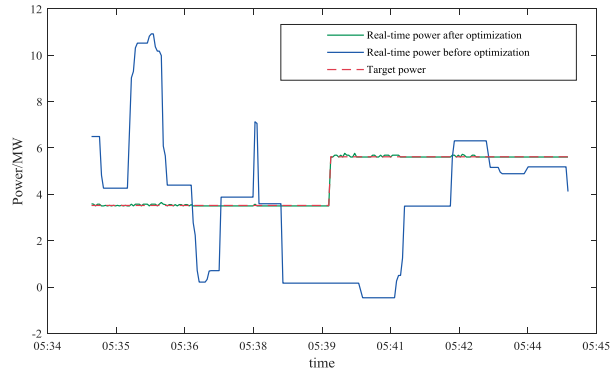

FIGURE 9. Schematic diagram of real-time power value tracking target power value.

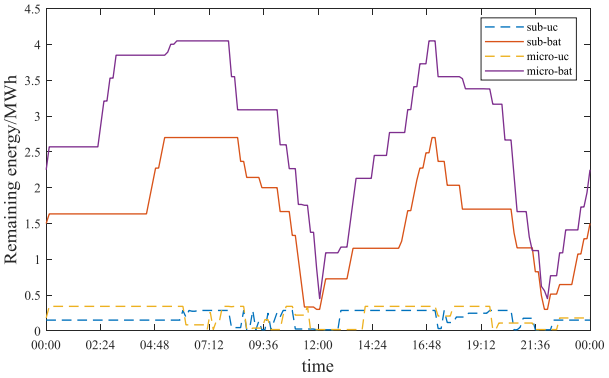

FIGURE 11. Schematic diagram of the state of charge change of each energy storage device.

negative power again. Besides, its overall load fluctuation has also been reduced.

A part of the results of real-time load tracking optimization is shown in Fig. 9. It can be seen that using real-time load tracking optimization can optimize the real-time power value to the target power value.

Fig. 10 shows the power required for the 10kV distribution network before and after optimization. It can be seen from Fig. 10 that the 10kV distribution network in FSTPSS can have less power supply pressure to a certain extent, and for users of the 10kV distribution network, their electricity bills have been reduced due to the cheaper electricity prices provided by the microgrid. Therefore, it is of practical significance to connect the 10kV distribution network to the microgrid along the railway.

The state of charge of each energy storage device is shown in Fig. 11. It can be seen from Fig. 11 that the increase in battery energy mainly occurs when the electricity price is low, and the decrease in battery energy mainly occurs when the electricity price is high. This is because the battery has a large capacity and a small instantaneous discharge power, and its main function is to save costs via energy arbitrage. The increase and decrease of capacitance energy are mainly occurs when the electricity price is high, and when the electricity price is low, capacitor energy hardly changes. This is because the capacitor has a small capacity and large instantaneous charging and discharging power. So usually, the main function of capacitors is not to store energy but to balance fluctuating loads. When the price of electricity is high, it is usually the peak period of electricity consumption. Therefore, capacitors need to be used frequently to balance the high fluctuations of the traction load.

Table 3 shows the operation costs of different types of TPSS. It can be seen from Table 3 that if the traditional TPSS traction substation is changed to the AC-DC-AC traction substation, the operation cost can be reduced by about 6%. This is mainly due to some functions of HESS in AC-DC-AC substation: First, the HESS in the AC-DC-AC traction substation can recuperate part of the energy from the regenerative braking of the train which could reduce electricity consumption costs. Second, HESS can use the electricity price difference to save electricity consumption costs. Thirdly, HESS could reduce peak power to save demand charge. And if the traditional TPSS is completely transformed into FSTPSS, it can cut the electricity costs by nearly half, because the FSTPSS system not only has the functions described above, but also has the function of acting as a micro power source. This ability is due to the distributed generation along the line connected to FSTPSS. Hence, the power consumed

TABLE 3. Comparison of operation costs of different types of TPSS.

	Traditional TPSS	TPSS with AC-DC-AC traction substation	FSTPSS
Daily operating cost (¥)	80125	75492	46334
Cost reduction	--	5.78%	42.17%

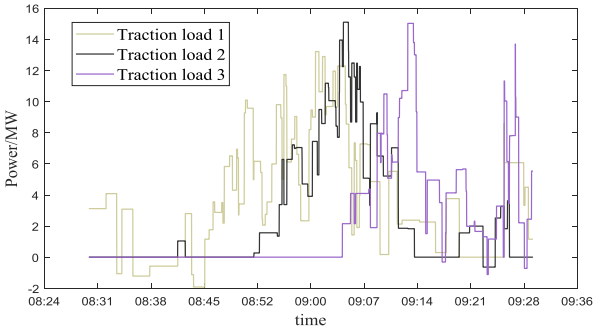

FIGURE 12. Diagram of the traction load of three FSTPSS units.

by the traction load is provided by distributed generation partly, which reduces electricity consumption cost. Therefore, in terms of daily operation costs, FSTPSS is the most economical.

B. CASE STUDY OF CENRTAL EMS

1) CASE DESCRIPTION

In this case, three consecutive FSTPSS units are considered. The train will pass through these three FSTPSS units in sequence. The traction load of these FSTPSS units is generated by the method described in [11]. Since the load generation method described in [11] takes into account the time sequence, the method can be extended to generate three consecutive traction loads. Specifically, the length of the power supply interval can be extended to three times, and then the loads of the three power supply intervals can be obtained sequentially in chronological order. Length of the power supply interval of each FSTPSS unit is set to 30km. The generated partial load curve is shown in Fig. 12.

The solar radiation data of the three FSTPSS units is obtained from [34]. And the power of PV generation of three FSTPSS units are shown in Fig. 13.

The load power of 10 kV distribution network of three FSTPSS units is shown in Fig. 14. The parameters of HESS, electricity consumption cost, electricity transmission cost, and demand charge are the same as the case above. The power transmission efficiency between adjacent FSTPSS units η is set to 0.968. η is calculated according to the traction power flow calculation software TRANS [41]–[43], which was developed by the Traction Power Supply Institute of Beijing Jiaotong University.

Before implementing the optimization goal of the central EMS, the optimization goal of the FSTPSS unit EMS

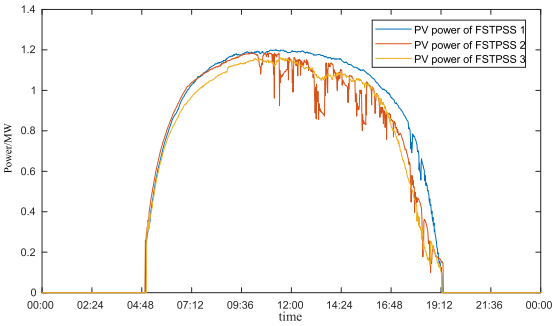

FIGURE 13. PV power of three FSTPSS units.

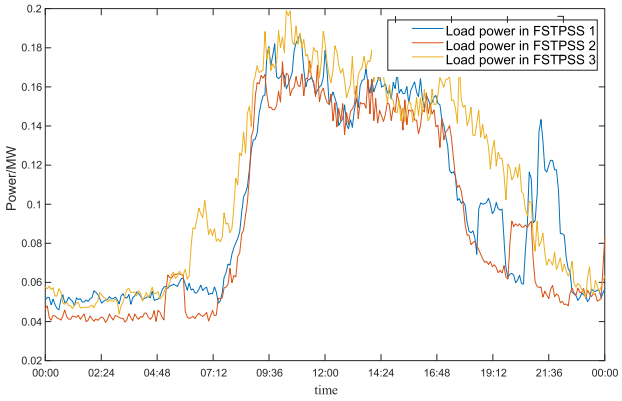

FIGURE 14. Load power of 10 kV distribution network.

is performed first. After that, according to the hierarchical sequence method, a specific cost margin is set for each FSTPSS unit so that the central EMS can complete its optimization goal. The margin of daily operation cost selected in this paper is ¥20,000 per FSTPSS unit.

2) OPERATION RESULT

The optimization problem of the whole FSTPSS is a mixed integer quadratic programming (MIQP) problem. The implementation process of the optimization algorithm is as follows: first, the optimal value of FSTPSS unit could be calculated according to its constraints and objective function; secondly, taking the optimal value of each FSTPSS unit plus its economic margin as the additional optimization constraints of the whole FSTPSS. Finally, optimal value of the whole FSTPSS can be calculated by YALMIP with CPLEX solver. The branch-and-cut method is used in solving MIQP by CPLEX solver.

The comparison of traction substation power before and after the optimization of central EMS is shown in Fig. 15. It can be seen that after the optimization of central EMS, the load fluctuation of each traction substation is significantly reduced.

The operation cost of each FSTPSS unit and the standard deviation of the traction substation power before and after optimization are shown in Table 4. From Table 4, it can be seen that the standard deviation of the traction

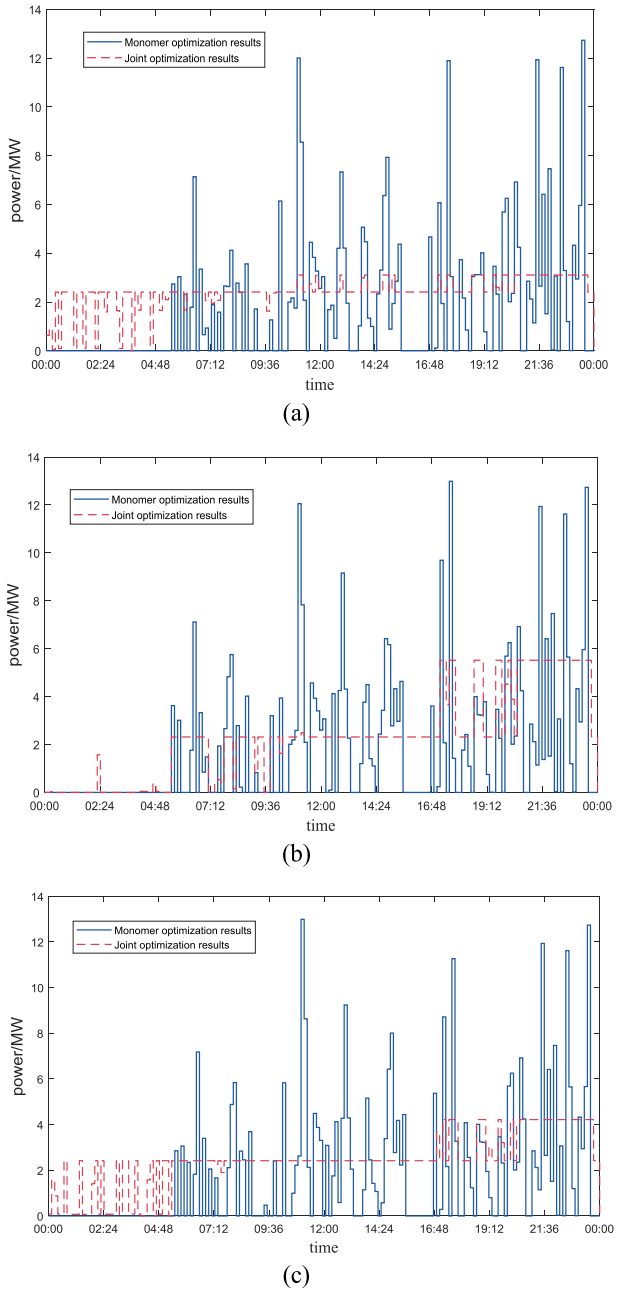

FIGURE 15. The comparison of traction substation power before and after the optimization of central EMS. (a)Power of traction substation of FSTPSS1. (b)Power of traction substation of FSTPSS2. (c)Power of traction substation of FSTPSS3.

substation power of each FSTPSS unit is significantly reduced after the optimization of the central EMS. However, its operation cost has increased after the optimization of the central EMS.

Therefore, reducing the volatility of the load has an associated cost. The increased daily operation cost of the FSTPSS unit can be understood as the cost paid to reduce the volatility of the load. Fig. 16 shows the relationship between the total daily operation cost of three FSTPSS units and the sum of the standard deviations of the traction substation power among these FSTPSS units.

TABLE 4. The operation cost of each FITPSS unit and the standard deviation of the traction substation power.

	FSTPSS1	FSTPSS2	FSTPSS3
Operating cost after monomer optimization (¥)	46334	47333	47554
Standard deviation (monomer optimization)	26.74	28.25	28.4
Operating cost after joint optimization (¥)	66334	67333	67554
Standard deviation (joint optimization)	4.53	17.02	9.5

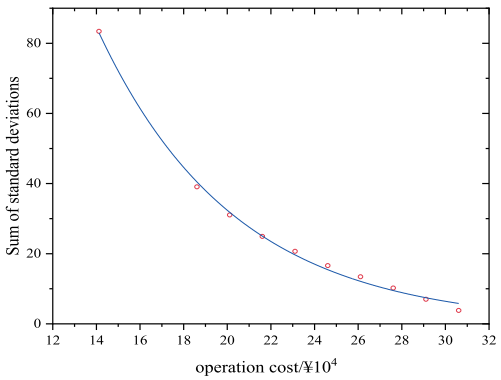

FIGURE 16. Schematic diagram of the relationship between daily operating loss and standard deviation of traction substation power.

If a negative exponential curve is used to fit it, the coefficient of determination reaches 0.997, and the fitting formula is shown in (28):

$$STD = 790.5e^{-\frac{C}{6.27}} - 0.177 \tag{28}$$

where C (¥10^4) is the operation cost of the three traction substations.

The central energy management system can select the appropriate operating mode according to this formula: load with less volatility or load with better economy.

C. PERFRMANCE ANALYSIS

Table 5 shows the computation time of the above optimization problem. Since the FSTPSS unit optimization and the whole FSTPSS optimization are day-ahead optimizations, their computation time are acceptable, and the computation time of real-time tracking optimization is less than its time interval of tracking (15s), its computation time is also acceptable in practical use. The computation time of the whole FSTPSS optimization is much higher than that of FSTPSS unit. The reason is that the whole FSTPSS optimization

TABLE 5. Computation time of each optimization problem.

Type	Computation time (s)
FSTPSS unit optimization	33.579
The whole FSTPSS optimization	952.262
Real-time tracking optimization	6.083

problem has excessive number of integer variables which makes the CPLEX solver have too many branches when using the branch-and-cut method. Too many branch variables make the computer's RAM not enough to be used. Therefore, the CPLEX solver calls the heuristic algorithm to reduce the number of branches. However, the heuristic algorithm cannot perform efficient parallel computing, so the computation time is greatly increased. In the future, if there are computers with larger RAM, this computation time can be significantly reduced.

In addition, since the long-distance transmission of current in the contact line has a huge loss, considering that the energy transmission efficiency is more than 90%, the joint optimized FSTPSS unit should not exceed four and the length of the whole FSTPSS should not exceed 120km. Also, due to the requirements of real-time operation, too many external random variables will also seriously affect the speed of real-time operation. Therefore, it is necessary to consider the computing performance of the computing device at the edge to comprehensively select the optimized number of variables. Concretely, the theoretical computation time for real-time tracking optimization should less than its time interval. According to the computation time of real-time tracking optimization, when three FSTPSS units are jointly optimized, the real-time tracking optimization time is 14.025s, and when four FSTPSS units are jointly optimized, the real-time tracking optimization time is 19.094s. Therefore, in this paper under the limitation of computer configuration, the number of optimized FSTPSS units should not exceed 3, but if the configuration of the computer is sufficient, the number of optimized FSTPSS units can reach 4. And due to the upper limit of the current carrying capacity of the contact wire of TPSS, the number of trains cannot be increased without limitation. According to [42], the current carrying capacity of a contact wire without a reinforced wire is 876A, so for a traction network with a voltage level of 27.5kV, its transmission capacity is 24.07MVA. The statistics in [11] show that the 90% power of a CRH2 train is about 5.8-6.5MW. Therefore, in order to ensure that the current carrying capacity of the contact line does not exceed its maximum value frequently, the number of trains in a FSTPSS unit should not exceed 4.

V. CONCLUSION

Many problems of traditional traction power supply systems are due to their inability to optimally control the flow of power. In this paper, a flexible smart traction power supply system (FSTPSS) is proposed. This traction power supply system can realize the smart control of the power of the entire electrified railway, and provides an interface for connecting distributed generation and distribution network.

In order to realize the flexible and smart control of the power of the entire electric railway, a hierarchical energy management strategy is proposed. This energy management strategy has two levels of optimization: FSTPSS unit EMS optimization and central EMS optimization. The optimization goal of the FSTPSS unit EMS is minimizing operation cost of unit throughout the day. The operating results show that the operating cost in the unit can be reduced by up to 42.17% compared with the traditional traction power supply system. After completing the optimal economic optimization of each FSTPSS unit, a certain economic margin is set for each FSTPSS unit to achieve the optimization of the central EMS. The optimization goal of the central EMS is to minimize the load fluctuation of the entire electrified railway. The optimized results show that the sum of the standard deviations of the power obtained by multiple FSTPSS units from the utility grid can continue to decrease as the economic margin increases. With an economic margin close to one-half of the operating cost, the sum of its standard deviations can be reduced by 62.8%. This paper also gives a specific formula for the relationship between sum of standard deviations and the overall railway operating cost. This formula can provide a reference for FSTPSS to select a suitable operating point.

At present, this novel topology traction power supply system has not been applied in practice. In the future, how to build this novel traction power supply system and whether the energy management strategy of this novel traction power supply system can be effectively implemented will be further studied.

REFERENCES

[1] S. Yang, X. Li, K. Song, and M. Wu, "A novel modeling approach of negative-sequence current for electrified railway traction substation," *Int. J. Electr. Power Energy Syst.*, vol. 107, pp. 462–471, May 2019.

[2] L. Li, M. Wu, S. Wu, J. Li, and K. Song, "A three-phase to single-phase AC-DC-AC topology based on multi-converter in AC electric railway application," *IEEE Access*, vol. 7, pp. 111539–111558, 2019.

[3] X. He, J. Peng, P. Han, Z. Liu, S. Gao, and P. Wang, "A novel advanced traction power supply system based on modular multilevel converter," *IEEE Access*, vol. 7, pp. 165018–165028, 2019.

[4] Z. Shu, S. Xie, K. Lu, Y. Zhao, X. Nan, D. Qiu, F. Zhou, S. Gao, and Q. Li, "Digital detection, control, and distribution system for co-phase traction power supply application," *IEEE Trans. Ind. Electron.*, vol. 60, no. 5, pp. 1831–1839, May 2013.

[5] H. Hayashiya, S. Kikuchi, K. Matsuura, M. Hino, M. Tojo, T. Kato, M. Ando, T. Oikawa, M. Kamata, and H. Munakata, "Possibility of energy saving by introducing energy conversion and energy storage technologies in traction power supply system," in *Proc. 15th Eur. Conf. Power Electron. Appl. (EPE)*, Sep. 2013, pp. 1–8.

[6] I. Sengor, H. C. Kilickiran, H. Akdemir, B. Kekezoglu, O. Erdinc, and J. P. S. Catalao, "Energy management of a smart railway station considering regenerative braking and stochastic behaviour of ESS and PV generation," *IEEE Trans. Sustain. Energy*, vol. 9, no. 3, pp. 1041–1050, Jul. 2018.

[7] J. Liu, W. Fang, X. Zhang, and C. Yang, "An improved photovoltaic power forecasting model with the assistance of aerosol index data," *IEEE Trans. Sustain. Energy*, vol. 6, no. 2, pp. 434–442, Apr. 2015.

[8] C. Wan, J. Lin, Y. Song, Z. Xu, and G. Yang, "Probabilistic forecasting of photovoltaic generation: An efficient statistical approach," *IEEE Trans. Power Syst.*, vol. 32, no. 3, pp. 2471–2472, May 2017.
[9] X. Yan, D. Abbes, and B. Francois, "Uncertainty analysis for day ahead power reserve quantification in an urban microgrid including PV generators," *Renew. Energy*, vol. 106, pp. 288–297, Jun. 2017.
[10] P.-H. Hsi and S.-L. Chen, "Electric load estimation techniques for high-speed railway (HSR) traction power systems," *IEEE Trans. Veh. Technol.*, vol. 50, no. 5, pp. 1260–1266, Sep. 2001.
[11] S. Yang, K. Song, and G. Zhu, "Stochastic process and simulation of traction load for high speed railways," *IEEE Access*, vol. 7, pp. 76049–76060, 2019.
[12] S. Singh, S. Hussain, and M. A. Bazaz, "Short term load forecasting using artificial neural network," in *Proc. 4th Int. Conf. Image Inf. Process. (ICIIP)*, 2017, pp. 1–5.
[13] Z. Li, S. Hoshina, N. Satake, and M. Nogi, "DC/DC converter development for battery energy storage supporting railway DC feeder system," in *Proc. 9th Int. Conf. Power Electron. ECCE Asia (ICPE-ECCE Asia)*, Seoul, South Korea, Jun. 2015, pp. 1655–1660.
[14] A. Ghazanfari, M. Hamzeh, and Y. Abdel-Rady I. Mohamed, "A resilient distributed decentralized control framework for DC parking lots," *IEEE Trans. Smart Grid*, vol. 9, no. 3, pp. 1930–1942, May 2018.
[15] H. A. Gabbar, A. M. Othman, and J. Chang, "Resilient interconnected microgrids for subway networks," in *Proc. Int. Conf. Renew. Energy Power Eng. (REPE)*, Nov. 2018, pp. 28–33.
[16] A. M. Othman and H. A. Gabbar, "Resilient interconnected microgrids (IMGs) with energy storage as integrated with local distribution networks for railway infrastructures," in *Proc. IEEE Smart Energy Grid Eng. (SEGE)*, Aug. 2016, pp. 170–174.
[17] T. Egan, H. A. Gabbar, A. M. Othman, and R. Milman, "Design and control of resilient interconnected microgrid for sustained railway," in *Proc. IEEE Int. Conf. Smart Energy Grid Eng. (SEGE)*, Aug. 2017, pp. 131–136.
[18] M. Chen, Z. Cheng, Y. Liu, Y. Cheng, and Z. Tian, "Multitime-scale optimal dispatch of railway FTPSS based on model predictive control," *IEEE Trans. Transport. Electrific.*, vol. 6, no. 2, pp. 808–820, Jun. 2020.
[19] S. Khayyam, F. Ponci, J. Goikoetxea, V. Recagno, V. Bagliano, and A. Monti, "Railway energy management system: Centralized–decentralized automation architecture," *IEEE Trans. Smart Grid*, vol. 7, no. 2, pp. 1164–1175, Mar. 2016.
[20] Y. Liu, M. Chen, S. Lu, Y. Chen, and Q. Li, "Optimized sizing and scheduling of hybrid energy storage systems for high-speed railway traction substations," *Energies*, vol. 11, no. 9, p. 2199, Aug. 2018.
[21] V. A. Kleftakis and N. D. Hatziargyriou, "Optimal control of reversible substations and wayside storage devices for voltage stabilization and energy savings in metro railway networks," *IEEE Trans. Transport. Electrific.*, vol. 5, no. 2, pp. 515–523, Jun. 2019.
[22] J. A. Aguado, A. J. S. Racero, and S. de la Torre, "Optimal operation of electric railways with renewable energy and electric storage systems," *IEEE Trans. Smart Grid*, vol. 9, no. 2, pp. 993–1001, Mar. 2018.
[23] P. Pankovits, J. Pouget, B. Robyns, F. Delhaye, and S. Brisset, "Towards railway-smartgrid: Energy management optimization for hybrid railway power substations," in *Proc. IEEE PES Innov. Smart Grid Technol., Eur.*, Oct. 2014, pp. 1–6.
[24] Y. Du and F. Li, "Intelligent multi-microgrid energy management based on deep neural network and model-free reinforcement learning," *IEEE Trans. Smart Grid*, vol. 11, no. 2, pp. 1066–1076, Mar. 2020.
[25] L. Che and M. Shahidehpour, "DC microgrids: Economic operation and enhancement of resilience by hierarchical control," *IEEE Trans. Smart Grid*, vol. 5, no. 5, pp. 2517–2526, Sep. 2014.
[26] X. Wu, Y. Xu, X. Wu, J. He, J. M. Guerrero, C.-C. Liu, K. P. Schneider, and D. T. Ton, "A two-layer distributed cooperative control method for islanded networked microgrid systems," *IEEE Trans. Smart Grid*, vol. 11, no. 2, pp. 942–957, Mar. 2020.
[27] H. Yang, W. Shen, Q. Yu, J. Liu, Y. Jiang, E. Ackom, and Z. Y. Dong, "Coordinated demand response of rail transit load and energy storage system considering driving comfort," *CSEE J. Power Energy Syst.*, vol. 6, no. 4, pp. 749–759, Dec. 2020.
[28] H. Novak, V. Lešić, and M. Vašak, "Hierarchical model predictive control for coordinated electric railway traction system energy management," *IEEE Trans. Intell. Transp. Syst.*, vol. 20, no. 7, pp. 2715–2727, Jul. 2019.
[29] L. Jiang, Z. Bie, T. Long, H. Xie, and Y. Xiao, "Distributed energy management of integrated electricity-thermal systems for high-speed railway traction grids and stations," *CSEE J. Power Energy Syst.*, early access, Oct. 6, 2020, doi: 10.17775/CSEEJPES.2020.02000.
[30] R. R. Kovacs and A. L. Leverett, "A load flow based method for calculating embedded, incremental and marginal cost of transmission capacity," *IEEE Trans. Power Syst.*, vol. 9, no. 1, pp. 272–278, Feb. 1994.
[31] J. Bialek, "Allocation of transmission supplementary charge to real and reactive loads," *IEEE Trans. Power Syst.*, vol. 13, no. 3, pp. 749–754, Aug. 1998.
[32] H. Rudnick, R. Palma, and J. E. Fernandez, "Marginal pricing and supplement cost allocation in transmission open access," *IEEE Trans. Power Syst.*, vol. 10, no. 2, pp. 1125–1132, May 1995.
[33] M. A. Mirzaei, M. Hemmati, K. Zare, B. Mohammadi-Ivatloo, M. Abapour, M. Marzband, and A. Farzamnia, "Two-stage robust-stochastic electricity market clearing considering mobile energy storage in rail transportation," *IEEE Access*, vol. 8, pp. 121780–121794, 2020.
[34] Y. Li, D. Han, and Z. Yan, "Long-term system load forecasting based on data-driven linear clustering method," *J. Mod. Power Syst. Clean Energy*, vol. 6, no. 2, pp. 306–316, Mar. 2018.
[35] National Renewable Energy Laboratory. *Measurement and Instrumentation Data Center*. Accessed: Jul. 1, 2020. [Online]. Available: https://midcdmz.nrel.gov/apps/sitehome.pl?site=BMS
[36] H. D. Chen, Y. An, and X. C. Meng, "Multi-objective optimal dispatching of microgrid based on improved genetic algorithm," in *Proc. 5th Int. Conf. Energy Mater. Environ. Eng. (ICEMEE)*, Kuala Lumpur, Malaysia, vol. 295, 2019, pp. 3–5.
[37] J. Loferg, "YALMIP: A toolbox for modeling and optimization in MATLAB," in *Proc. IEEE Int. Conf. Robot. Automat.*, New Orleans, LA, USA, Sep. 2004, pp. 284–289.
[38] *IBM ILOG CPLEX Optimization StudioV12.10.0 Documentation*. Accessed: Jan. 22, 2021. [Online]. Available: https://www.ibm.com/support/knowledgecenter/zh/SSSA5P_12.10.0/COS_KC_home.html
[39] M. Barros and M. Casquilho, "Linear programming with CPLEX: An illustrative application over the Internet CPLEX in fortran 90," in *Proc. 14th Iberian Conf. Inf. Syst. Technol. (CISTI)*, Coimbra, Portugal, Jun. 2019, pp. 1–6.
[40] L. Sun, W. Liu, B. Xu, and T. Chai, "The scheduling of steel-making and continuous casting process using branch and cut method via CPLEX optimization," in *Proc. 5th Int. Conf. Comput. Sci. Converg. Inf. Technol.*, Seoul, South Korea, Nov. 2010, pp. 716–721.
[41] J. Zhang, M. Wu, and Q. Liu, "A novel power flow algorithm for traction power supply systems based on the Thévenin equivalent," *Energies*, vol. 11, no. 1, p. 126, Jan. 2018.
[42] J. Zhang and W. Mingli, "Method for OCS current capacity calculation in AC railways," in *Proc. IEEE Conf. Expo Transp. Electrific. Asia–Pacific (ITEC Asia–Pacific)*, Beijing, China, Aug. 2014, pp. 1–6.
[43] W. Mingli and F. Yu, "Numerical calculations of internal impedance of solid and tubular cylindrical conductors under large parameters," *IEE Proc.-Gener., Transmiss. Distrib.*, vol. 151, no. 1, p. 67, 2004.

YICHEN YING (Student Member, IEEE) was born in Zhejiang, China, in 1996. He received the B.S. degree in electrical engineering from the University of South China, Hengyang, China, in 2017. He is currently pursuing the Ph.D. degree in electrical engineering with Beijing Jiaotong University, Beijing, China. His research interests include power flow calculation and energy management of traction power supply systems.

QIUJIANG LIU (Member, IEEE) was born in Hebei, China. He received the B.Sc., M.Sc., and Ph.D. degrees in electrical engineering from Beijing Jiaotong University (BJTU), Beijing, China, in 2012, 2014, and 2018, respectively. He is currently a Postdoctoral Researcher with BJTU. His research interests include power quality of electric railways, energy storage systems, and other applications of power electronics in traction power supply systems.

MINGLI WU (Member, IEEE) was born in Hebei, China, in November 1971. He received the B.S. and M.S. degrees in electrical engineering from Southwest Jiaotong University, Chengdu, China, in 1993 and 1996, respectively, and the Ph.D. degree in electrical engineering from Beijing Jiaotong University, Beijing, China, in 2006. Since 2008, he has been a Professor with the School of Electrical Engineering, Beijing Jiaotong University. His current research interests include power supplies for electric railways, digital simulation of power systems, and electric power quality.

YATING ZHAI (Student Member, IEEE) was born in Hebei, China. She received the M.Sc. degree from Shijiazhuang Tiedao University, in 2017. She is currently pursuing the Ph.D. degree in electrical engineering with Beijing Jiaotong University. Her research interests include power supply for electric railways, electromagnetic transient theory, and simulation for electric railway traction power supply systems.